Hierarchical Graphene-Based Films with Dynamic Self-Stiffening for Biomimetic Artificial Muscle

Zhaohe Dai, Yanlei Wang, Luqi Liu, Xuelu Liu, PingHeng Tan, Zhiping Xu,* Jun Kuang, Qing Liu, Jun Lou, and Zhong Zhang**

Biological tissues such as muscle cells can adapt their structural and mechanical response upon external mechanical stimuli. Conversely, artificial muscles, intended to reproduce the salient functional features of biological muscles, usually undergo mechanical fatigue when subjected to dynamic stress. Besides passively improving the resilience to dynamic loads, here, it is reported that macroscopic films based on graphene and its chemical derivate exhibit an increase in modulus by up to 84% after subjected to a low-amplitude (0.1%) dynamic tension. Through a combination of experimental testing and molecular dynamics simulations, the unique self-stiffening behavior is attributed to the straightening and reorientation of graphene sheets and is further tuned through tailoring interlayer adhesion. Meanwhile, artificial muscles based on graphene films are designed and interestingly improved stiffness of our muscle materials after "training" are demonstrated. These results help to harness the stiffening mechanism and can be useful for the development of adaptable structural materials for biomechanical applications.

1. Introduction

Natural muscles are adaptive materials with hierarchical structure driven by a complex mechanism and are capable of production of large strain with fast response time, moderate stress, and long lifetime. Well-known adaptive behaviors include muscle cell remodeling and strengthening through changing actin cytoskeleton and other cellular processes in response to various strains.[1] Artificial muscles are intended to reproduce the salient functional features of biological muscles.[2] However, different from the way that biological tissues response to external stresses, the man-made materials generally response passively due to lack of structural complexity. Consequently, most synthetic muscles, when subjected to dynamic stress, will under microstructural damage even though the strain is performed within the low strain level they could bear. While major advances in artificial muscle materials with improving mechanical resilience have been obtained in the last few years,[3–6] design and introduction of adaptive hierarchical architectures in synthetic materials to achieve self-stiffening behavior observed in biotissues is an alternative and fascinating route to approach repeated loading resistance.[7,8]

Over the past decade, research works have proven that various nanocarbon materials based macroscopic architectures have endowed the materials with biomimetic performance.[3–6] Moreover, the outstanding mechanical properties of carbon nanostructures could elevate the response significantly, and their multifunctional performance offers a new dimension in responsive material design.[9] Here, we report that graphene and/or its chemical derivate graphene oxide (GO) based free-standing film materials increase in stiffness up to 64% when subjected to a low-amplitude (0.1%) dynamic tension. This dynamic self-stiffening behavior is a unique and not-yet-observed phenomenon in various carbon nanostructured macroscopic architectures and may be useful to the understanding and development of adaptive structural materials based on nanocarbon materials. Additionally, extensive works have utilized graphene-based films as artificial muscles materials and most of them focused on the electrical properties and actuation performances.[10,11] Our findings indicate that rich behavior of graphene films during dynamic actuation strain enables the design of graphene-based artificial muscle to not only generate deformation but also display self-stiffening in response to dynamic stresses like natural muscles.

Z. Dai, Prof. L. Liu, J. Kuang, Q. Liu, Prof. Z. Zhang
CAS Key Laboratory of Nanosystem and Hierarchical Fabrication
CAS Center for Excellence in Nanoscience
National Center for Nanoscience and Technology
Beijing 100190, China
E-mail: liulq@nanoctr.cn; zhong.zhang@nanoctr.cn
Z. Dai, X. Liu, J. Kuang, Q. Liu
University of Chinese Academy of Science
Beijing 100049, China
Y. Wang, Prof. Z. Xu, Prof. Z. Zhang
Applied Mechanics Laboratory
Department of Engineering Mechanics and Center for Nano and Micro Mechanics
Tsinghua University
Beijing 100084, China
E-mail: xuzp@tsinghua.edu.cn
X. Liu, Prof. P. H. Tan
State Key Laboratory of Superlattices and Microstructures
Institute of Semiconductors
Chinese Academy of Sciences
Beijing 100083, China
Prof. J. Lou
Department of Materials Science and NanoEngineering
Rice University
Houston, TX 77005, USA

DOI: 10.1002/adfm.201503917

© 2016 WILEY-VCH Verlag GmbH & Co. KGaA, Weinheim

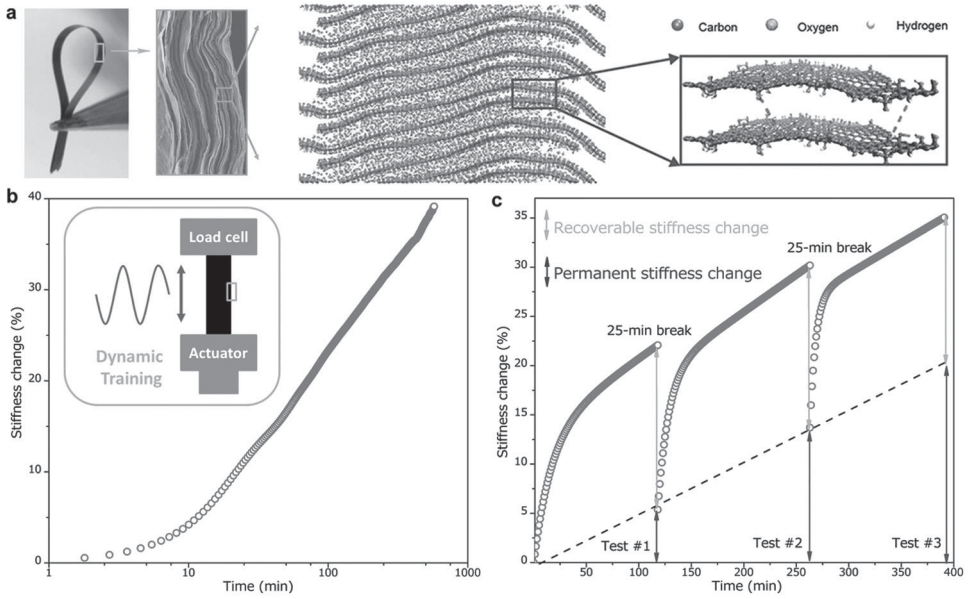

Figure 1. Structural features and self-stiffening behavior of GO films. a) From left to right: digital picture of flexible strip specimen; SEM side-view image of the micrometer-scale curved structures in GO film; schematic for nanoscale microstructures, where oxygen-rich groups are functionalized on graphene sheet, leading to corrugated morphologies, hydrophilic surfaces, and an interfacial gallery open for various intersheet bonding types. b) The specimens display change in stiffness (%) versus time when dynamically stretched at 10 μm amplitude, 1 Hz, 35 °C, a preload of 0.01 N using a DMA Q800 (inset). c) 25 min breaks without any loading were performed during dynamic tests, indicating recoverability of stiffness changes during dynamic stress. The recoverable change is labeled as gray arrows and could be recovered completely within 25 min (Supporting Information Figure S2), and the black arrows represent permanent stiffness changes.

GO nanosheets are synthesized from natural graphite powder via chemical exfoliation.[12] Owing to its atomic thickness and chemical functionalities on the surface, the individual graphene platelets behave high flexibility and present intrinsic wrinkling and wavy microstructures at different length scale.[13] Such features still remained in macroscopic materials (e.g., GO films in **Figure 1**a), which enable them to remodel in response to external dynamic strain.[14] Herein, we examine the response of GO films to low-amplitude (0.1%) dynamic tension, and dynamic self-stiffening behavior is seen to continue leading to a discernible increase in stiffness and modulus after thousands of cycles. Through a combination of dynamic mechanical testing (DMA), polarized Raman spectroscopy, X-ray diffraction (XRD), and molecular dynamics (MD) simulations, we attribute the self-stiffening behavior to the evolution of hierarchical microstructure graphene assembled, including straightening and reorientation of graphene nanosheets during dynamic loading. Furthermore, we designed electrothermal air pump artificial muscles by utilization of layered graphene films as heating elements and demonstrated unusual self-stiffening behavior on the stiffness of our artificial muscle materials after "training," similar to the strength training process in human muscles.

2. Results and Discussions

2.1. Observation of Self-Stiffening in GO Films

The macroscopic GO films were fabricated by the flow-directed filtration method and specimens were cut by a razor blade into strips before further tests as shown in Figure 1a.[5,15–17] Dynamic mechanical testing may introduce failure into most synthetic materials due to fatigue (under repeated tension or compression even though the strain applied is significantly lower than the level they could bear under monotonically loading conditions). Alternatively, Figure 1b shows GO film displays an increasing stiffness up to 40% in response to 10 μm amplitude dynamic tensile deformation. Moreover, there is no observable upper limit to this behavior after even 10 h of continuous dynamic strain, indicating that there is potential for even greater improvement. Testing at various frequencies also exhibited the similar effect, implying that the self-stiffening behavior is independent of the special experimental parameters used. Instead, it is closely related to the microstructural evolution of hierarchical layered structures in GO Films during dynamic loading process that will be discussed later. Similar to that in previously reported strain hardening behavior observed in polymer nanocomposites and liquid crystal elastomers under dynamic compression,[7,8] such microstructure-evolution-caused phenomenon in GO films could only be effectively actuated under dynamic loading, as the static load testing revealed no increase in the stiffness change in Supporting Information Figure S1a. Nevertheless, unlike the obvious dimensional changes before and after dynamic compression in previous works,[7,8] the changes in our samples is quite negligible due to low-amplitude tensile strain (≈0.1%) utilized as shown in Supporting Information Figure S1b.

After exploring the influence of dynamic and static stress on the observation of self-stiffening behavior, the materials were then tested with several breaks (without any stress) during

© 2016 WILEY-VCH Verlag GmbH & Co. KGaA, Weinheim

dynamic loads to ascertain whether or not the increased stiffness could be preserved in the absence of external loads. As shown in Figure 1c and Supporting Information Figure S2a, the stiffness change between each dynamic test begins at a little lower value than the end point of the previous one, but it quickly resumes the path from earlier test. Since this drop could be observed in each break between dynamic tests, we presume that the increase in stiffness is partially recoverable. This recoverability is also explored in samples that rested for different time during dynamic tests in Supporting Information Figure S2b, indicating that the recoverable improved stiffness could recover completely within 25 min. Moreover, the unrecovered (permanent) stiffness change in our samples shows continuous increase over time when they are dynamically stressed (dash line in Figure 1c). Furthermore, such dynamic stress caused stiffness change is associated with an increased resistance to static deformation. Thus, the application of low-strain, repetitive tension represents a facile method to improve the Young's modulus of graphene-based film materials, which are typically improved by modifying divalent ions or introducing crosslink into adjacent sheets.[16,18,19] The static tensile properties of various graphene-based films before and after dynamic tension are tested in Supporting Information Figure S3 and summarized in **Table 1** and Supporting Information Table S1 (the detail will be discussed later).

2.2. Self-Stiffening Mechanism and Microstructural Analysis

Self-reinforcing behavior is well known for polymer materials in which macromolecular movements (e.g., straightening and reorientation) would improve the alignment as well as original stiffness of curved and unaligned polymer chains at large strain level.[20,21] Similarly, our filtration-fabricated GO films also showed highly curved and partially aligned microstructures as shown in Figure 1a. Suspended individual GO sheets are unavoidably corrugated due to their atomic thickness and the irregular distribution of oxygen-rich groups on the surface as well as thermal fluctuation.[22] When corrugated sheets are assembled together on the porous filter membrane, a curved structure is formed in which GO sheets could not completely align along the same direction.[23] When GO film is subjected to a unidirectional dynamically tension, the movements of graphene nanosheets could be easily actuated, which would induce the structural evolution and improve the original stiffness.

Herein, we characterize the microstructural evolution of GO films during dynamical tension via typically used Raman spectra technique.[20,24] Polarized Raman spectra were recorded by using an incident laser beam parallel to the base plane of the dynamically stressed and unstressed GO films. As shown in **Figure 2**a, the angle (θ) between the electric field vector of the incident laser and the base plane of the GO film is tuned from 0° to 360° with a step of 20°. The *G*-band intensity depends on the angle (θ) and ($I_G(\theta)$) was theoretically analyzed in Supporting Information Figure S4. $I_G(\theta)$ reaches a maximum ($I_G(\parallel)$) when the electric field vector of the incident laser is parallel to the base plane of the GO film ($\theta = 0°$ and 180°), whereas $I_G(\theta)$ reaches a minimum ($I_G(\perp)$) when the electric field vector of the incident laser is normal to the base plane of the GO film ($\theta = 90°$ and 270°). The ratio $I_G(\parallel)/I_G(\perp)$ is equal to $\cot^2\alpha$ and exhibits an increasing tendency with decreasing α, where α is the alignment angle between average GO nanosheets and loading or length direction, as shown in Figure 2b. For both stressed and unstressed samples, the experimental $I_G(\theta)$ decreases gradually when θ varies from 0° to 90°. However, the $I_G(\parallel)/I_G(\perp)$ changes from 3.4 for unstressed samples to 5.0 for dynamically stressed films, indicating the improvement on alignments of the graphene sheet along loading (length) direction after dynamic stressing. Similar behavior has also been found before for carbon nanotube or graphene-based nanocomposites.[20,24] Specifically, as shown in Figure 2b, the nanosheets in unstressed samples could be considered to be averagely distributed at 28.3° with respect to the loading direction. By contrast, distribution angle of graphene decreased to 24.1° for dynamically stressed samples, implying that microstructural evolution occurred and caused improved alignments during dynamic tension.

To further shed light on the microstructural evolution of graphene nanosheets and its stiffening mechanism, we simplified possible movements of GO sheets on the basis of MD simulation. First, similar to that observed in polymer chains,[20,21] the straightening movements of highly curved structure of GO sheets were remarkable under tension loading. In addition to improving the sheets alignments, the reduction in curved profiles also increases the contact area between neighboring sheets and hence offers better stress transfer capacity under external loads (Figure 2c, details in Supporting Information

Table 1. Dynamic and static properties of nanosheet-based films.

Sample	*d*-spacing [nm]	Young's modulus before stressed [GPa]	Young's modulus after stressed[a)] [GPa]	Change in modulus [%]	Change In stiffness[b)] [%]	Change In toughness [%]
A-GO	0.68	14.2	15.8	12	24	3
W-GO	0.75	6.2	11.4	84	64	–55
W-Re-GO	0.38	5.4	6.5	20	26	–9
W-GA-GO[c)]	1.17	13.6	21.0	54	16	–2
Nanoclay	NM	6.4	7.9	23	34	–10

A, as-prepared; *W*, H_2O-treated; *Re*, reduced; *GA*, glutaraldehyde-treated; NM, not measured; [a)]Young's modulus: measured after ≈2 h dynamic tension; [b)]Stiffness change: measured by DMA under dynamic tensile strain after ≈2 h dynamic tension; [c)]Note that water-treated *GA*-GO sample (*W-GA*-GO) exhibits the highest value in the modulus after stressing among all the samples as shown in Figure S3c and Table S1 (Supporting Information).

© 2016 WILEY-VCH Verlag GmbH & Co. KGaA, Weinheim

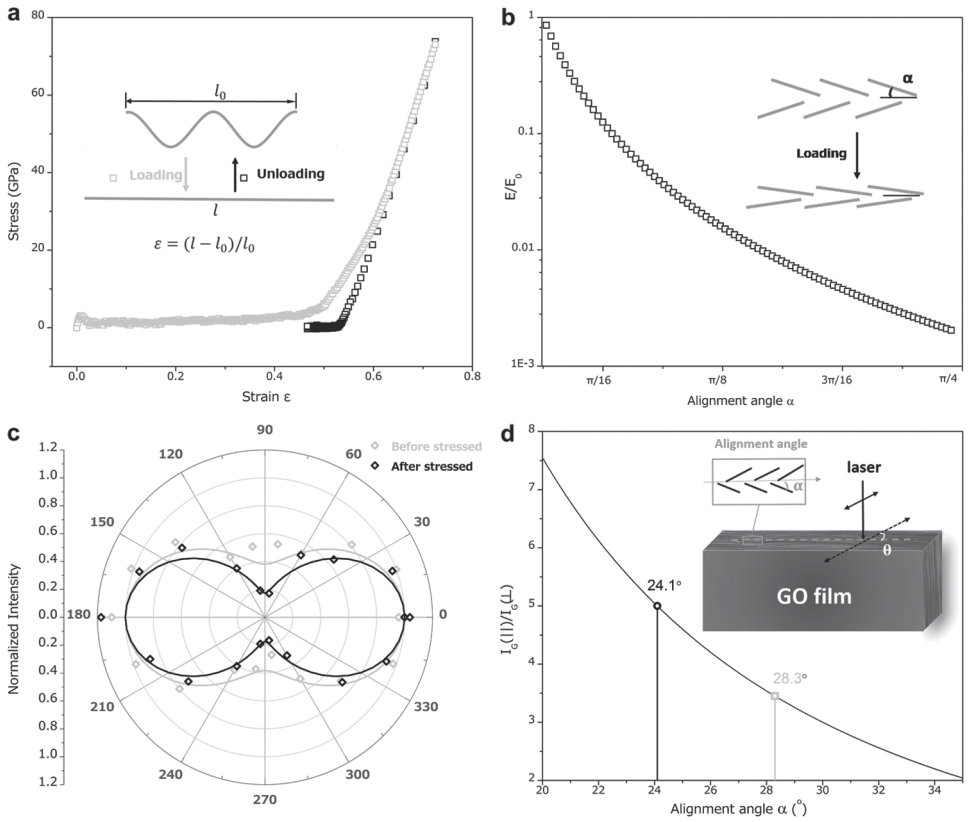

Figure 2. Microstructural analysis of GO films. a) The G band intensity, $I_G(\theta)$, as a function of the angle θ between the electric field vector of the incident laser and the base plane of the GO film for stress (black diamonds and black fitting curves) and unstressed samples (gray diamonds and the gray fitting curves). b) The ratio $I_G(\|)/I_G(\perp)$ as a function of the alignment angle α. The fitted data in (b) are indicated. Inset: schematic illustration of the measurement geometry of the Raman analysis for stress or unstressed GO films. c) Straightening of highly curved GO sheet stacked in GO films displays nonlinearly stiffening response. Curved GO sheet will be stretched to be flat one under the external loads and the contacting area of neighboring sheets will increase and hence lead to a higher effective Young's modulus. d) Preferred alignment of GO sheets to the loading direction effectively elevates the stiffness (E/E_o) of the films. These aligned GO sheets would be difficult to return to the original state due to the cohesion between neighboring sheets and redistribution of water molecules in the interlayer gallery.

Figure S5). Meanwhile, the resulted stiffness increase can be gradually restored over time after unloading in Figure 2a, we thus speculate that the recoverable stiffness change observed in Figure 1c might be related to the such straightening movements of nanosheets. Second, the reorientation movements of unaligned and partially aligned graphene nanosheets could also be observed. Moreover, when the misaligned GO sheets could be along the loading direction, a mechanically stiffer sample is achieved due to directly improved alignment of the 2D lamellar structures (Figure 2b and Supporting Information Figure S6 for a detailed and quantified explanation).[25]

2.3. Tuning Self-Stiffening Behavior by Tailoring Interlayer Adhesions

The interlayer movement has been considered as the origin of the dynamic self-stiffening behavior in GO films. We thus tried to tune the interlayer adhesion in efforts to further understand and tailor the movements of nanosheets as well as the self-stiffening behavior for such graphene-based film materials. Our earlier works have proven that it is possible to tailor the interfacial adhesions of GO-based film materials through introducing small molecules into neighboring GO nanosheets.[16] Herein, molecular-level tuning of the interlayer properties as well as self-stiffening behavior of GO sheets is utilized. First, H_2O treatment is employed to tune the interfacial H-bonding interactions in order to facilitate the self-stiffening performance. Due to their rotational degrees of freedom that water molecules can break and reform new hydrogen bond to the external load, accelerating the reorientation of GO sheets along the loading direction.[16,19,26] Glutaraldehyde (GA) was also introduced to the gallery regions of the GO film to create covalent bonding between neighboring GO sheets, which could introduce the multimodal crosslinking (hydrogen bonding and covalent bonding interaction) and, in turn, improve their bulk mechanical properties.[16] As a comparison, hydroiodic (HI) aqueous solution was used to prepare the chemically reduced GO (*Re*-GO) film with mainly Van der waals (Vdw) interactions.

FTIR spectra are used to characterize the chemical modification of GO film (see Supporting Information Figure S7). The XRD patterns in **Figure 3**a indicate the intercalation of GA molecules into the gallery space and reduction of GO sheets. The slightly increased *d*-spacing for all samples after water treatment

© 2016 WILEY-VCH Verlag GmbH & Co. KGaA, Weinheim

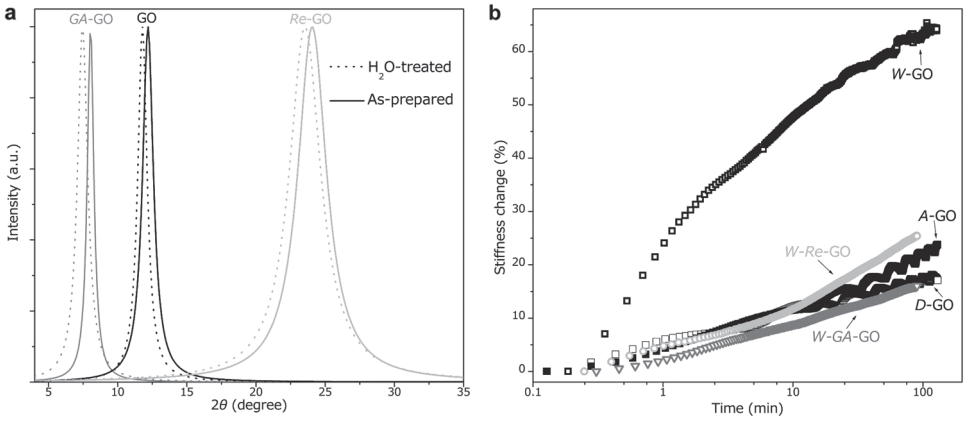

Figure 3. Tuning the interlayer adhesion of graphene-based films as well as their self-stiffening performance. a) XRD patterns of the GO, *Re*-GO, and *GA*-GO films. The slightly increased *d*-spacing for all samples illustrates the successful intercalation of water inside the gallery space. b) The dynamic response versus stressing time of GO, *Re*-GO, and *GA*-GO films. More details in various sample and their static tensile properties before and after dynamic process are shown in Supporting Information Figure S3. Note about the sample name: *A,* as-prepared; *W,* H_2O-treated; *Re,* reduced; *GA,* Glutaraldehyde-treated.

illustrates the successful intercalation of water inside the gallery space. The response of GO film (H-bonding interaction), *Re*-GO film (mainly Vdw interaction), and *GA*-GO film (multimodal crosslinking) to dynamic tension is shown in Figure 3b, S3 and summarized in S1 (Supporting Information), where *W* means H_2O-treated, *Re* means reduced, and *GA* means glutaraldehyde-treated. As expected, all samples treated by interlayer H-bonding interactions show more significant improvement in the dynamic stiffness compared to ones without water treatment. Particularly, as shown in Figure 3b and S1 (Supporting Information), up to 64% stiffness change could be observed in *W*-GO films with H-bonding interaction. Further static tensile results of various graphene-based films before and after dynamic treatment show similar trend in Young's modulus changes with ones derived from dynamical tests (Table 1, S1 and Supporting Information Figure S3 insets). Particularly, dynamically stressed *W*-GO films shows as high as 84% increase in modulus (from 6.2 to 11.4 GPa) compared to unstressed samples, while the toughness of the graphene films show decrease to some extent due to the reduction of failure strain after dynamic tension. The differences in the enhancement of Young's modulus and stiffness might be related to dynamical measurements of the stiffness, which is influenced by the viscoelastic properties of samples. On the other hand, besides of its positive effects, the H-bonding tuning also exhibited negative effects on modulus improvements because introduction of H-bonding into interlayer gallery would increase the *d*-spacing of graphene-based films (Figure 3a) and hence typically weakened the samples in modulus.[16] Similar with the results of our previous work,[16] the water-treated (tuning the H-bonding interaction) samples typically showed lower modulus compared to ones without water treatment as shown in Supporting Information Table S1. However, benefiting from positive effects of H-bonding on the dynamic self-stiffening performance, our *W-GA*-GO films showed the highest value in the modulus (≈21 GPa) after dynamic stressing among all the samples, exhibiting the potential of utilizing the self-stiffening behavior to improve the Young's modulus of graphene-based film materials in future.

2.4. Graphene-Based Artificial Muscles with Biomimetic Self-Stiffening Behavior

Regular elastic stress on biological tissues such as bones and muscles will stimulate a localized structural remodeling, a response mechanism commonly referred to as Wolff's law,[27] which reduces the risk of failure in areas of frequent loading. From biomimetic perspective, the self-stiffening response to cyclic loads in graphene-based films might be important, as the adaptive movements of the graphene sheets induced by external mechanical stimuli should prove to be a powerful tool to maintaining mechanical stability. Herein, in addition to observe and clarify self-stiffening behavior in these nanolayered materials, we also employ them as artificial muscles due to this biomimetic feature. Based on our previous work, an electrothermal air pump-type artificial muscle was fabricated by utilization of *Re*-GO films as heating element to transfer electrical stimulus into mechanical energy.[5] **Figure 4**a shows the actuation strain profile of *Re*-GO film along the midline under actuated state. The actuation mechanism is related to the Joule heating induced expansion of the sealed air under electric stimulus. Our actuators exhibit repeatable, stable cyclic actuation under a 5 V driving voltage as shown in Figure 4b. The displacement could be maintained and recovered during the cyclic actuation process for more than 1400 cycles (4 h at 0.1 Hz), indicating the long time working life of this nanostructured carbon materials based pump actuator. More interestingly, like strength training in human muscles, the stiffness of our artificial muscles, as quantified by modulus in Figure 4c, show about 15% improvement after 4 h exercising (actuating). While numbers of works have been done to fabricate graphene-based artificial muscles with high actuation performance such as large actuation displacement, high energy density and fast response time and so on,[4,11,28] no reports addressing the design of artificial muscles with biomimetic self-stiffening behavior exist. Therefore, this intriguing behavior not only gives new insight into the graphene sheets movements in bulk materials, but could be utilized to design

© 2016 WILEY-VCH Verlag GmbH & Co. KGaA, Weinheim

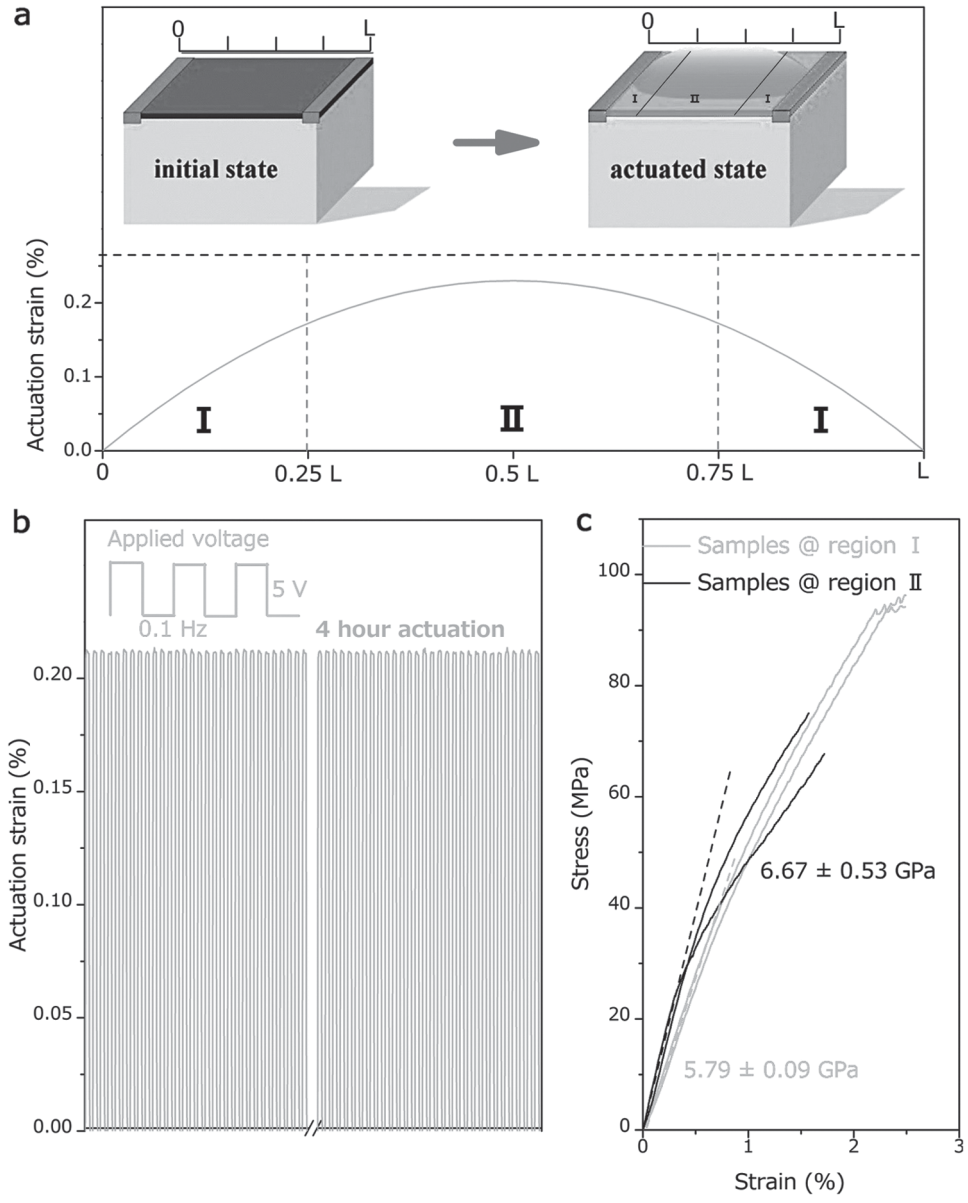

Figure 4. The actuation performance testing of artificial muscles. a) Depiction of the initial and actuated state of an air pump-type electrothermal actuator. b) Cyclic actuation strain under a 5 V driving voltage. The displacement was measured by using laser displacement sensor and concentrating on the center of films. c) The stress–strain curves of the *Re*-GO films cut from region I (gray, negligible actuation strain) and region II (black, ≈0.1%–0.2% strain) after 4 h dynamic actuation.

artificial muscles which could noninvasively, unconsciously improve their stiffness during use.

As above-mentioned, the self-stiffening behavior in our graphene-based film materials should be attributed to the microstructural movements of the nanosheets in response to external dynamic loading, which fundamentally are originated from high flexibility of graphene and hierarchical multi-scale wrinkling microstructures they assembled. We thus surmised that various kinds of flexible nanoplate-based macroscopic films could exhibit such adaptive behavior if they could be hierarchically structured in a similar manner as graphene films. Herein, the response of nanoclay-based films to the same dynamic strain is examined in Supporting Information Figure S8 and excitingly, 34% change in stiffness and 23% increase in Young's modulus is observed after 100 min repeated tension. Recently, it was also observed in 3D bundled actin networks under cyclic shear and liquid crystal elastomers under repeated compression, which attributed to the reorganization of the network constituents and reorientation of mobile nematic directors, respectively.[8,29] It is reasonable to conclude that, the key for the design of self-stiffening materials is the introduction of hierarchy with the ability to remodeling and reorganizing into microstructure. And recent progresses in preparing various types of graphene (or nanoscale building blocks more broadly)

© 2016 WILEY-VCH Verlag GmbH & Co. KGaA, Weinheim

based macroscopic architectures has demonstrated that it has become possible to design macroscopic materials with desired hierarchical nanostructures for a large range of applications.[30] While most of applications require the materials with dynamic mechanical stability, besides passively improving the resilience to dynamic loads, the design and introduction of adaptive hierarchical microstructures in synthetic materials to achieve self-stiffening behavior is an alternative and fascinating route.

3. Conclusion

In summary, we report the self-stiffening behavior of macroscopic GO films in response to dynamic strain with as high as 84% increase in modulus, which has not been previously reported for carbon nanostructure based macroscopic materials. Combination of MD simulations and experimental results show that reorientation of GO sheets along the loading direction occurs during dynamic process. This self-stiffening behavior is further tuned though tailoring interlayer adhesions between graphene sheets and utilized to design artificial muscles. Our results will help to understand self-stiffening mechanism and utilize these special adaptive microstructures for the development of novel self-stiffening, high-performance, and flexible materials for artificial biomaterials.

4. Experimental Section

Preparation of Graphene-Based Films: GO, *GA*-GO, and *Re*-GO films were prepared according to previous works.[5,6,16,17] GO films were made by filtration of the resulting colloid (10 mL) through a cellulose membrane filter (47 mm in diameter, 0.22 μm pore size), followed by air drying and peeling from the filter. As-prepared GO films were dried at 60 °C for 12 h with a vacuum oven. *Re*-GO films could be obtained by dipping GO films in an HI aqueous solution (25%) at 80 °C for 10 min, and then washing repeatedly with ethanol to remove the residual HI. The treatment with *GA* was performed by exposure to *GA* vapors for 6–8 h at 37 °C to prepare *GA*-GO films. To study the hydration behavior of them, the H_2O-treated samples were placed in an environmental chamber (EYEL4, KCL 2000) at a relative humidity of 60% and 30 °C for 2 d. Samples of GO (≈6 μm thick), *GA*-GO (≈10 μm thick), and *Re*-GO film (≈3 μm thick) prepared in this manner were cut by a razor blade into strips (20×2 mm^2) before further tests.

Characterization: The cross section of specimen was studied by field-emission SEM (HITACHI S-4800). Spectral analysis was characterized by FTIR spectroscopy (Spectrum One, PE, US). XRD measurements for film samples were performed at room temperature using specular reflection mode (Cu KR radiation, X'Pert PRO, PANalytical, Holland). Raman measurements were used to analyze the orientation of GO sheets before and after dynamic stressing. The polarized Raman spectra were collected in the back scattering geometry using a Jobin-Yvon HR800 micro-Raman system equipped with a liquid-nitrogen-cooled charge couple detector, a X100 objective lens (numerical aperture ≈0.90), and a 600 lines mm^{-1} grating. The excitation wavelength is 633 nm from an He–Ne laser. A motorized x–y stage and a rotational stage were used to vary the films angle with respect to the vector of the linearly polarized excitation.

Mechanical Testing: A dynamic mechanical analyzer (TA, DMA Q800) was employed to evaluate the mechanical performances of GO film. The static tensile tests were conducted in displacement ramp mode with a prestrain 0.01% and a ramp rate of 0.2% μm min^{-1}. Dynamic tension testing as illustrated in Figure 1a was conducted at 10 μm amplitude (0.1% strain), 1 Hz, 35 °C, a preload of 0.01 N. In static load testing, the samples were subjected to the constant load identical to those used for dynamic testing, which is fundamentally a creep testing. All tests were conducted isothermally at 35 °C (unless otherwise noted).

Preparation of Pump-Type Artificial Muscles: The artificial muscles were prepared as following: polytetrafluoroethylene boxes (length × width × depth is $15 \times 15 \times 10$ mm^3) with one end open were first machined, and then graphene films were glued onto the top of the boxes to seal the air inside. Two pieces of copper conductive strips were pasted on the films as electrodes. The electrical power was supplied using a Tektronix Arbitrary Function Generator (AFG3011), and the displacement was measured using a LK-G5001 laser displacement sensor. The actuation mechanism was related to the Joule heating induced expansion of the sealed air in the boxes under electric stimulus. The laser was concentrated on the center of the carbon material films to detect the displacement change. The temperature of the materials when the actuation deformation reached the maximum during the actuation process was measured using a laser sight infrared thermometer in a previous work.[5]

MD Simulations: MD simulations were performed by using the large-scale atomic/molecular massively parallel simulator package.[31] For detailed information, see Supporting Information Methods. For all simulations, a model GO with hydroxyl groups functionalized on the graphene sheet was considered, where a typical number concentrations n_C:n_O:n_H = 1:0.1:0.1.

Supporting Information

Supporting Information is available from the Wiley Online Library or from the author.

Acknowledgements

This project was jointly supported by the National Key Basic Research Program of China (Grant Nos. 2012CB937503 and 2013CB934203) and the National Natural Science Foundation of China (Grant Nos. 51173030, 11225210, 21474023, 11222217, 11225421, 11434010 and 11474277).

Received: September 15, 2015
Revised: March 23, 2016
Published online: August 16, 2016

[1] R. De, A. Zemel, S. A. Safran, *Nat. Phys.* **2007**, *3*, 655.
[2] Y. Bar-Cohen, *Electroactive Polymer (EAP) Actuators as Artificial Muscles: Reality, Potential, and Challenges*, Vol. *5*, SPIE Press, Bellingham, WA **2004**.
[3] R. H. Baughman, C. Cui, A. A. Zakhidov, Z. Iqbal, J. N. Barisci, G. M. Spinks, G. G. Wallace, A. Mazzoldi, D. De Rossi, A. G. Rinzler, *Science* **1999**, *284*, 1340.
[4] T. Mirfakhrai, J. D. Madden, R. H. Baughman, *Mater. Today* **2007**, *10*, 30.
[5] Q. Liu, L. Liu, J. Kuang, Z. Dai, J. Han, Z. Zhang, *Nanoscale* **2014**, *6*, 6932.
[6] Q. Liu, L. Liu, K. Xie, Y. Meng, H. Wu, G. Wang, Z. Dai, Z. Wei, Z. Zhang, *J. Mater. Chem. A* **2015**, *3*, 8380.
[7] B. J. Carey, P. K. Patra, L. Ci, G. G. Silva, P. M. Ajayan, *ACS Nano* **2011**, *5*, 2715.
[8] A. Agrawal, A. C. Chipara, Y. Shamoo, P. K. Patra, B. J. Carey, P. M. Ajayan, W. G. Chapman, R. Verduzco, *Nat. Commun.* **2013**, *4*, 1739.
[9] a) M. Falvo, G. Clary, R. Taylor, V. Chi, F. Brooks, S. Washburn, R. Superfine, *Nature* **1997**, *389*, 582; b) C. Lee, X. Wei, J. W. Kysar, J. Hone, *Science* **2008**, *321*, 385.

© 2016 WILEY-VCH Verlag GmbH & Co. KGaA, Weinheim

[10] a) J. Liang, Y. Huang, J. Oh, M. Kozlov, D. Sui, S. Fang, R. H. Baughman, Y. Ma, Y. Chen, *Adv. Funct. Mater.* **2011**, *21*, 3778; b) G. W. Rogers, J. Z. Liu, *J. Am. Chem. Soc.* **2011**, *134*, 1250; c) J. Liang, L. Huang, N. Li, Y. Huang, Y. Wu, S. Fang, J. Oh, M. Kozlov, Y. Ma, F. Li, *ACS Nano* **2012**, *6*, 4508; d) J.-H. Jeon, R. K. Cheedarala, C.-D. Kee, I.-K. Oh, *Adv. Funct. Mater.* **2013**, *23*, 6007; e) J. Zang, S. Ryu, N. Pugno, Q. Wang, Q. Tu, M. J. Buehler, X. Zhao, *Nat. Mater.* **2013**, *12*, 321.
[11] a) J. Kim, J.-H. Jeon, H.-J. Kim, H. Lim, I.-K. Oh, *ACS Nano* **2014**, *8*, 2986; b) L. Kong, W. Chen, *Adv. Mater.* **2014**, *26*, 1025.
[12] W. S. Hummers Jr., R. E. Offeman, *J. Am. Chem. Soc.* **1958**, *80*, 1339.
[13] L. Qiu, X. Zhang, W. Yang, Y. Wang, G. P. Simon, D. Li, *Chem. Commun.* **2011**, *47*, 5810.
[14] X. Shen, X. Lin, N. Yousefi, J. Jia, J.-K. Kim, *Carbon* **2014**, *66*, 84.
[15] D. A. Dikin, S. Stankovich, E. J. Zimney, R. D. Piner, G. H. Dommett, G. Evmenenko, S. T. Nguyen, R. S. Ruoff, *Nature* **2007**, *448*, 457.
[16] Y. Gao, L. Q. Liu, S. Z. Zu, K. Peng, D. Zhou, B. H. Han, Z. Zhang, *ACS Nano* **2011**, *5*, 2134.
[17] L. Liu, Y. Gao, Q. Liu, J. Kuang, D. Zhou, S. Ju, B. Han, Z. Zhang, *Small* **2013**, *9*, 2466.
[18] S. Park, K.-S. Lee, G. Bozoklu, W. Cai, S. T. Nguyen, R. S. Ruoff, *ACS Nano* **2008**, *2*, 572.
[19] O. C. Compton, S. W. Cranford, K. W. Putz, Z. An, L. C. Brinson, M. J. Buehler, S. T. Nguyen, *ACS Nano* **2012**, *6*, 2008.
[20] Z. H. Dai, Y. Gao, L. Q. Liu, P. Potschke, J. L. Yang, Z. Zhang, *Polymer* **2013**, *54*, 3723.
[21] R. Haward, *Macromolecules* **1993**, *26*, 5860.
[22] Z. Xu, M. J. Buehler, *ACS Nano* **2010**, *4*, 3869.
[23] X. Yang, L. Qiu, C. Cheng, Y. Wu, Z. F. Ma, D. Li, *Angew. Chem., Int. Ed.* **2011**, *50*, 7325.
[24] a) Q. Liang, X. Yao, W. Wang, Y. Liu, C. P. Wong, *ACS Nano* **2011**, *5*, 2392; b) Z. Li, R. J. Young, I. A. Kinloch, *ACS Appl. Mater. Interfaces* **2013**, *5*, 456.
[25] a) Y. Liu, B. Xie, Z. Xu, *J. Mater. Chem.* **2011**, *21*, 6707; b) Y. L. Liu, B. Xie, Z. Zhang, Q. S. Zheng, Z. P. Xu, *J. Mech. Phys. Solids* **2012**, *60*, 591.
[26] a) Y. J. Su, H. Wei, R. G. Gao, Z. Yang, J. Zhang, Z. H. Zhong, Y. F. Zhang, *Carbon* **2012**, *50*, 2804; b) N. V. Medhekar, A. Ramasubramaniam, R. S. Ruoff, V. B. Shenoy, *ACS Nano* **2010**, *4*, 2300.
[27] A. Chamay, P. Tschantz, *J. Biomech.* **1972**, *5*, 173.
[28] a) L. Lu, J. Liu, Y. Hu, Y. Zhang, H. Randriamahazaka, W. Chen, *Adv. Mater.* **2012**, *24*, 4317; b) K. Chung, S. Yu, C. J. Heo, J. W. Shim, S. M. Yang, M. G. Han, H. S. Lee, Y. Jin, S. Y. Lee, N. Park, *Adv. Mater.* **2012**. *24*, 2375.
[29] K. M. Schmoller, P. Fernandez, R. C. Arevalo, D. L. Blair, A. R. Bausch, *Nat. Commun.* **2010**, *1*, 134.
[30] a) Z. Niu, J. Chen, H. H. Hng, J. Ma, X. Chen, *Adv. Mater.* **2012**, *24*, 4144; b) Y. Wu, N. Yi, L. Huang, T. Zhang, S. Fang, H. Chang, N. Li, J. Oh, J. A. Lee, M. Kozlov, A. C. Chipara, H. Terrones, P. Xiao, G. Long, Y. Huang, F. Zhang, L. Zhang, X. Lepró, C. Haines, M. D. Lima, N. P. Lopez, L. P. Rajukumar, A. L. Elias, S. Feng, S. J. Kim, N. T. Narayanan, P. M. Ajayan, M. Terrones, A. Aliev, P. Chu, Z. Zhang, R. H. Baughman, Y. Chen, *Nat. Commun.* **2015**, *6*, 6141; c) X. l. Huang, D. Xu, S. Yuan, D. l. Ma, S. Wang, H. y. Zheng, X. b. Zhang, *Adv. Mater.* **2014**, *26*, 7264; d) X. Yu, B. Lu, Z. Xu, *Adv. Mater.* **2014**, *26*, 1044; e) Q. Liang, Z. Li, X. Yu, Z. H. Huang, F. Kang, Q. H. Yang, *Adv. Mater.* **2015**, *27*, 4634; f) S. Yao, Y. Zhu, *Adv. Mater.* **2015**, *27*, 1480; g) Z. Dai, L. Liu, X. Qi, J. Kuang, Y. Wei, H. Zhu, Z. Zhang, *Sci. Rep.* **2016**, *6*, 18930.
[31] S. Plimpton, *J. Comput. Phys.* **1995**, *117*, 1.

© 2016 WILEY-VCH Verlag GmbH & Co. KGaA, Weinheim